atmosphere

MDPI

Article

Investigating the Sensitivity of Modelled Ozone Levels in the Mediterranean to Dry Deposition Parameters

André Barreirinha [1], Sabine Banzhaf [2], Markus Thürkow [2], Carla Gama [1], Michael Russo [1], Enrico Dammers [3], Martijn Schaap [2,3] and Alexandra Monteiro [1,*]

[1] CESAM and Department of Environment and Planning, University of Aveiro, 3810-193 Aveiro, Portugal; andre.barreirinha@ua.pt (A.B.); carlagama@ua.pt (C.G.); michaelarusso@ua.pt (M.R.)
[2] Institute of Meteorology, Freie Universität Berlin, 14195 Berlin, Germany; sabine.banzhaf@met.fu-berlin.de (S.B.); markus.thuerkow@met.fu-berlin.de (M.T.); martijn.schaap@tno.nl (M.S.)
[3] Air Quality and Emissions Research, Netherlands Organisation for Applied Scientific Research (TNO), 3508 TA Utrecht, The Netherlands; enrico.dammers@tno.nl
* Correspondence: alexandra.monteiro@ua.pt

Abstract: The exposure to elevated levels of ozone contributes to respiratory diseases and ecosystem degradation. Mediterranean countries are among those most affected by high ozone concentrations, which are generally overestimated by chemistry transport models underscoring the importance of improving the accuracy of air quality modelling. This study introduces an enhanced Mediterranean dry deposition description within the LOTOS-EUROS model framework, focusing on refining key vegetation parameters for the Mediterranean climate zone, with the goal to better estimate deposition and connected concentration values. Adjustments were made to the vegetation type dependent Jarvis functions for temperature and vapour pressure deficit, as well as to the maximum stomatal conductance across four land use types: arable land, crops, deciduous broadleaf forest, and coniferous evergreen forest. The model's baseline run showed a widespread overestimation of ozone. Adjustments to the dry deposition routines reduced this overestimation, but the model simulation incorporating all changes still showed elevated ozone levels. Both runs displayed moderate spatial correlation with observations from 117 rural background monitoring stations, and most stations exhibited a temporal correlation between 0.5 and 0.8. An improved RMSE and bias were noted at the majority of the stations (114 out of 117) for the model simulation incorporating all changes. The monthly analysis indicated consistent overestimation at two Portuguese sites beginning in March. The model effectively tracked temporal changes overall. However, the diurnal analysis revealed site-specific differences: an overestimation at the station closest to highly populated areas at night, while rural stations aligned better with observed values. These results highlight the benefits of region-specific model adaptations and lay the groundwork for further advancements, such as incorporating detailed vegetation classifications and seasonal variations.

Keywords: ozone; chemistry transport model; dry deposition; Portugal

Academic Editor: Giacomo Alessandro Gerosa

Received: 24 March 2025
Revised: 10 May 2025
Accepted: 13 May 2025
Published: 19 May 2025

Citation: Barreirinha, A.; Banzhaf, S.; Thürkow, M.; Gama, C.; Russo, M.; Dammers, E.; Schaap, M.; Monteiro, A. Investigating the Sensitivity of Modelled Ozone Levels in the Mediterranean to Dry Deposition Parameters. *Atmosphere* **2025**, *16*, 620. https://doi.org/10.3390/atmos16050620

Correction Statement: This article has been republished with a minor change. The change does not affect the scientific content of the article and further details are available within the backmatter of the website version of this article.

1. Introduction

Ozone (O_3) is a critical component of atmospheric chemistry with significant implications for both ecosystems and human health [1,2]. Elevated ozone levels can cause respiratory diseases, reduce lung function, and exacerbate conditions such as asthma [3,4]. For ecosystems, ozone acts as a phytotoxic pollutant, impairing photosynthesis, reducing

crop yields, and affecting forest health [5,6]. Ozone concentration values are particularly relevant in Southern European countries due to their warm climate, intense sunlight [7], and frequent atmospheric stagnation [8], which enhance photochemical reactions that generate ground-level ozone from a combination of short and long-lived organic compounds and nitrogen oxides (NO_x) emitted by traffic, industry, and other anthropogenic sources [9,10]. Portugal, one of these European Southern countries, frequently registers exceedances to the legislated threshold values at the few rural stations spread over the country [11,12]. Ambient ozone levels negatively influence the quantity and quality of wine production, an essential economic sector in the country [13].

Due to the limited number of monitoring stations, air quality models—using atmospheric physics, chemistry, and emissions data—are necessary to help estimate pollutant concentrations across broader areas, filling gaps in spatial coverage. The accurate modelling of ozone and its deposition is essential for understanding its distribution and impacts. Recent studies under the Air Quality Model Evaluation International Initiative (AQMEII) have highlighted persistent issues with ozone concentration overestimation in regional air quality models [14]. These overestimations lead to inaccurate assessments of ozone exposure and its effects. Improving the representation of deposition processes and refining model parameters to better reflect real-world conditions can potentially reduce this overestimation of modelling results and improve model accuracy. There is currently no model fully adapted to the Mediterranean climate, although some models, such as EMEP, have already implemented some vegetation-specific parameters for Mediterranean climates [15]. Since deposition related challenges concerning eutrophication and acidification are more pronounced in other countries, such as the Netherlands and Germany, the current deposition models have been developed with the specific vegetation of these countries in mind [16–18]. These state-of-the-art chemistry transport models (CTMs) employ the widely used resistance approach to estimate deposition velocities and then calculate the deposition flux over each grid cell and/or land use.

This paper aims to better represent ozone distributions across Portugal by improving deposition rates across the Mediterranean region, and at the same time to develop a first working version of an improved Mediterranean deposition module for the LOTOS-EUROS (LOng Term Ozone Simulation—EURopean Operational Smog) modelling system. Through sensitivity simulations, we aim to understand which parameters drive the changes in modelled ozone concentrations and depositions. By achieving these objectives, this study aims to enhance the accuracy of ozone modelling in Portugal and the Mediterranean region as a whole, providing a more reliable basis for assessing the impacts of ozone on natural ecosystems, crop production, and human health.

The paper is organised as follows. Section 2 describes the methodology followed, namely the CTM modelling system, its dry deposition module, and the sensitivity simulations performed. Section 3 presents the results obtained for different deposition parameters and explains the ozone concentration values (modelled and observed over the Mediterranean). Section 4 summarises and concludes the results of this study.

2. Methodology

2.1. Chemistry Transport Modelling with LOTOS-EUROS

The LOTOS-EUROS chemistry transport model is a three-dimensional Eulerian model developed for regional air quality assessments and operational forecasts across Europe [19]. It enables the modelling of dispersion, chemical reactions, and deposition of atmospheric pollutants, including both gases and aerosols. LOTOS-EUROS has been widely used for ozone applications across Europe (e.g., [20,21]). It has also been applied on the national scale, including Germany [22] and Spain [23] and worldwide, like in Asia [24]. LOTOS-

EUROS is part of the Copernicus Atmospheric Monitoring Service (CAMS) European air quality ensemble [25]. This service uses a number of advanced CTMs to operationally forecast the concentrations of criteria air pollutants. Within CAMS, LOTOS-EUROS is regularly validated against in situ observations and satellite data. It also has been compared with other models in multi-model intercomparison studies and typically demonstrates robust performance [14,22,26–29]. For a more detailed description of the model and its input data, please refer to Manders et al. [19].

In this study, the LOTOS-EUROS model version 2.3 was applied to simulate ozone distributions for the year 2021. The model domain covers most of the Mediterranean (13° W–26° E; 30–46° N) with a resolution of 21 × 21 km^2 (Figure 1). The 21 × 21 km^2 resolution provides a good balance between computational cost and spatial detail. Although the rather low resolution might lead to a more homogenous spatial distribution pattern of the modelled concentrations, it still captures the general ozone concentration in the regional background [30]. The resolution is also well suited to capture the changes made in the deposition of ozone that were performed in this study (see Section 3.2). The model has been driven by meteorological data sourced from the ECMWF (European Centre for Medium-Range Weather Forecasts) short-term forecast system, providing a 3-hourly temporal resolution that is subsequently interpolated to an hourly frequency within the model. We make use of a high vertical resolution to better capture the mixing in the planetary boundary layer. Compared to the earlier used mixing layer approach described in Manders et al. [19], the higher resolved vertical layering leads to a better model performance, as shown by Escudero et al. [23]. The simulations were performed using 12 vertical levels, ranging from the ground up to approximately 10 km above the Earth's surface, aligning with a combination of the layering from the ECMWF meteorology datasets. Gridded emission inventories are utilised at both European and national scales, sourced from the CAMS regional inventory (CAMS-REG) v5.1 (TNO version). The emission inventory contains several emission sources, such as shipping, road transport, residential heating, and others. Natural emissions of sea spray, dust, and biogenic VOCs (volatile organic compounds) are highly sensitive to meteorological conditions and, for that reason, are computed directly within the model, following the meteorology dependent parameterizations described in Manders et al. [19] and the references therein. The emissions are time-allocated using hourly factors for different aggregated source categories. Fire emissions are obtained from the CAMS Global Fire Assimilation System (GFAS) product [31].

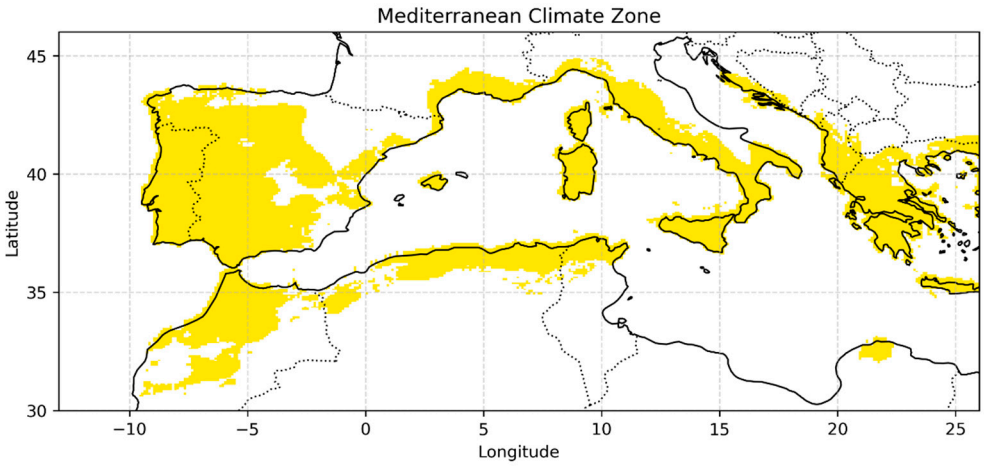

Figure 1. Modelling domain and Mediterranean climate zone as defined in the LOTOS-EUROS model (highlighted in yellow).

2.2. Dry Deposition Parameterization

The land use type influences the dry deposition characteristics of atmospheric species. LOTOS-EUROS uses the Corine 2018 Land Cover Database [32], which is enhanced by the distribution of 115 tree species [33]. The grid cells in LOTOS-EUROS are defined by the fraction of each land use present in that cell [19].

LOTOS-EUROS uses the DEPosition of Acidifying Compounds (DEPAC) module to calculate the dry deposition [34]. This module is based on Erisman et al. [35]. It employs the widely used resistance analogy, which contains three different resistances: aerodynamic resistance (R_a), quasi-laminar sublayer resistance (R_b), and surface resistance (R_c). R_a depends only on meteorology and surface roughness, R_b depends on canopy height and wind speed, while the surface term R_c is the most complex as it is divided into vegetated and non-vegetated pathways. The R_c non-vegetated pathway only includes the soil resistance, which varies depending on whether the soil is frozen, wet, or dry. Meanwhile, the vegetated pathway is subdivided into three other pathways. Up first is the vegetated soil pathway, which includes the soil resistance and an in-canopy resistance. The leaf cuticle pathway consists of a resistance that varies depending on whether the surface is wet or dry. Finally, the stomata pathway is considered, which includes the stomatal resistance. With these resistances, the dry deposition flux (F_{dry}) can be calculated with Equation (1).

$$F_{h,dry} = V_d * C_h \tag{1}$$

where C_h is the concentration at height h and V_d is the deposition velocity that can be calculated from the resistances with Equation (2).

$$V_d = (R_a + R_b + R_c)^{-1} \tag{2}$$

Several studies have acknowledged that warmer climate conditions are linked to increased stomatal conductance (e.g., [36–38]). The vegetation parameters used in the LOTOS-EUROS dry deposition routine are based on north-western European process studies in temperate climates. As our study area experiences significantly higher temperatures than temperate climates, this study focuses on the stomatal conductance of O_3. These higher temperatures in this region are expected to impact ozone deposition fluxes and concentrations.

The stomatal conductance is modelled using a land-use-specific maximum stomatal conductance, which is lowered by empirically derived functions that describe the closure of the stomata, namely the so-called Jarvis functions:

$$g_{sto} = g_{max} * \left[min\left(f_{phen}, f_{O3}\right)\right] * f_{light} * \max\left\{f_{min}, \left(f_{temp} * f_{VPD} * f_{SW}\right)\right\} \tag{3}$$

Several vegetation parameters driving the stomatal conductance were tested, such as the minimum, optimal, and maximum temperatures at which the stomata is open (T_{min}, T_{opt} and T_{max}, respectively), the maximum and minimum vapour pressure deficit (VPD_{max} and VPD_{min}), the minimum stomatal conductance (f_{min}), and the species-specific maximum stomatal conductance (g_{max}). T_{min}, T_{opt}, and T_{max} are used to calculate the Jarvis function for temperature (f_{temp}), as described by Equation (4).

$$f_{temp} = max\left\{\left[(T - T_{min})/(T_{opt} - T_{min})\right] * \left[(T_{max} - T)/(T_{max} - T_{opt})\right]^{bt}\right\} \tag{4}$$

The relation between f_{temp} and g_{sto} is described in Figure 2 (left panel). For temperatures below T_{min} or above T_{max}, the relative stomata conductance is 0, meaning the stomata are fully closed and do not capture any O_3. Changing T_{min} to lower values and/or T_{max} to

larger values would cause the stomata to be open for a larger span of conditions, allowing vegetation to absorb more O_3, which prompts a decrease in O_3 concentrations [39].

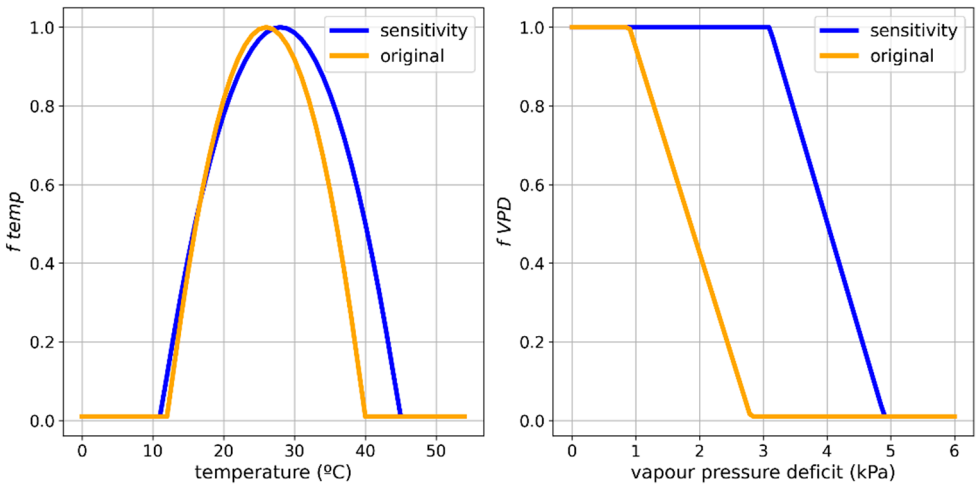

Figure 2. Example of the impact of the changes made for arable land use in the Jarvis functions for temperature (**left**) and vapour pressure deficit (**right**).

Another impactful variable in the stomatal conductance is the vapour pressure deficit, which is described by Equation (5).

$$f_{VPD} = \left\{1, max\left\{f_{min}, \left((1 - f_{min}) \times \frac{VPD_{min} - VPD}{VPD_{min} + VPD_{max}}\right) + f_{min}\right\}\right\} \quad (5)$$

The relation between f_{VPD} and g_{sto} is presented in Figure 2 (right panel), where the example for arable land exemplifies that by adapting these values to the vegetation in a Mediterranean climate, the stomata will be open for more extended periods. This occurs because Mediterranean vegetation is more accustomed to lower humidity. By increasing the VPD_{max} value, we increase the time window where the stomata are fully open (relative g_{sto} = 1). If VPD on the surface increases past the VPD_{max}, the stomata start to close, and when VPD reaches the value for VPD_{min}, it fully closes.

2.3. Sensitivity Runs and Parameter Updates

The values for the vegetation parameters tested (f_{temp}, f_{VPD} and g_{max}) were taken from the International Cooperative Programme Vegetation in chapter 3 [39]. These include the Mediterranean Needleleaf, Mediterranean Broadleaf, Mediterranean Crop and Durum Wheat, which correspond to Coniferous Evergreen Forest (FCE), Broadleaf Deciduous Forest (FBD), Crops (CRP) and Arable Land (ARA) in the LOTOS-EUROS model. Table 1 presents the updated values under Mediterranean (med) and the default values under Temperate (tmp).

Table 1. Values updated in the stomatal conductance equation for the Mediterranean climate zone. Values for the original (Temperate, tmp) and the modified LOTOS-EUROS (Mediterranean, med).

	T_{min}		T_{opt}		T_{max}		VPD_{min}		VPD_{max}		g_{max}	
	tmp	**med**	**tmp**	**med**	**tmp**	**med**	**tmp**	**med**	**tmp**	**med**	**tmp**	**med**
ARA	12	11	26	28	40	45	2.8	4.9	0.9	3.1	300	410
CRP	12	13	26	28	40	39	2.8	4.6	0.9	3.2	300	782
FBD	0	0	20	22	35	35	3.25	3.1	1	1.1	150	265
FCE	0	1	18	23	36	39	3	4	0.5	2.2	140	195

To assess the impact of the changes, 13 runs in addition to the baseline case were conducted in this study. For each of the four land uses, three individual runs were made: one focused on the changes to the maximum stomatal conductance, another on the changes to the temperature Jarvis function, and the third on the changes to the vapour pressure deficit Jarvis function. Each of these runs can be identified as {land use}-{change} (e.g., the sensitivity run for the changes in f_{temp} in arable land can be identified as ARA-f_{temp}). Finally, a run with all changes for all land uses (i.e., all-changes run) has been performed.

2.4. Evaluation Metrics and Measurement Data

The model output for ozone includes simulated concentration distributions (surface level and all vertical layers) along with the dry deposition fluxes. This study focused on ozone dry deposition and concentration outputs. The period between April and September 2021 was chosen to compare the model with observations, as this is the most relevant period for ozone photochemical production. Observational data on the ozone concentration were obtained from the European air quality database. Due to the 21 × 21 km^2 resolution, only rural background stations were used to compare our model results to. The nearest neighbour interpolation method was used to select one model grid cell per station. Stations above 700 m were excluded from the analysis as these stations are often located in the free troposphere, and the evaluation results will be biased towards the ability to correctly assess whether the station is in the boundary layer or not. Only stations with at least 75% data availability for 2021 were considered. In total, 117 sites were used to validate the model simulations for O_3, and 106 sites were used to compare the model results with the observations for nitrogen dioxide (NO_2). For the model validation, the mean NO_2 values and the mean daily maximum eight-hour average (MDA8) of ozone were calculated for the study period at each station. For the statistical analysis, the Pearson correlation, RMSE, and bias were calculated.

In some parts of the analysis, the stations were restricted to the Portuguese domain due to the well-documented high ozone concentrations in the country [40,41], as well as the known overestimation of ozone by the models over Portugal (e.g., [13,42]). Two of the stations, Santa-Combinha (SCO) and Lourinhã (LNH), were selected for further evaluation. For these two stations, the closest model grid cell has a high percentage of the land use classes that have been adapted to the Mediterranean climate. The grid cell for the Santa-Combinha station is composed of 25% ARA, 38% CRP, 11% FBD and 2% FCE, totalling 76% of these land use classes. The grid cell for Lourinhã consists of 28% ARA, 28% CRP, 16% FBD, and 1% FCE, totalling 73%.

3. Results and Discussion

3.1. Modelled Ozone Concentration

Figure 3 shows the map of the MDA8 for ozone of the baseline simulation averaged over the study period. Mean MDA8 of O_3 observed values are shown as dots on the map.

The MDA8 of O_3 over the Mediterranean Sea is significantly higher than those modelled inland due to several key factors. Firstly, inland ozone undergoes deposition over soil and vegetation, which effectively reduces its atmospheric concentration. In contrast, the deposition rate over the sea is considerably lower, allowing ozone to accumulate and persist at higher levels. Secondly, the lifetime for many pollutants is longer across the sea, causing effective photochemistry to take place. Over the mainland, the modelled MDA8 of O_3 concentrations show higher values in the surroundings of highly populated areas such as large cities in Southern Spain (Barcelona, Murcia, Granada, Malaga) and the Po Valley in Italy. This may be linked to substantial NOx emissions from traffic and industrial activities in the adjacent cities. The highest NO_2 values are modelled along the

main shipping routes and larger cities, which leads to the destruction of ozone, reducing its concentration (see Supplementary Materials). In urban environments, high concentration values of NO_2 were modelled and observed during the main rush hour, initiated by NO emissions from traffic and residential combustion. The lowest NO_2 concentration is modelled at noon and at night, where anthropogenic NO emissions are lower. Ozone formation in rural areas usually tends to be NOx-limited due to the scarcity of traffic and industrial emissions. However, due to the proximity to larger cities, some may experience lower ozone concentrations [43,44].

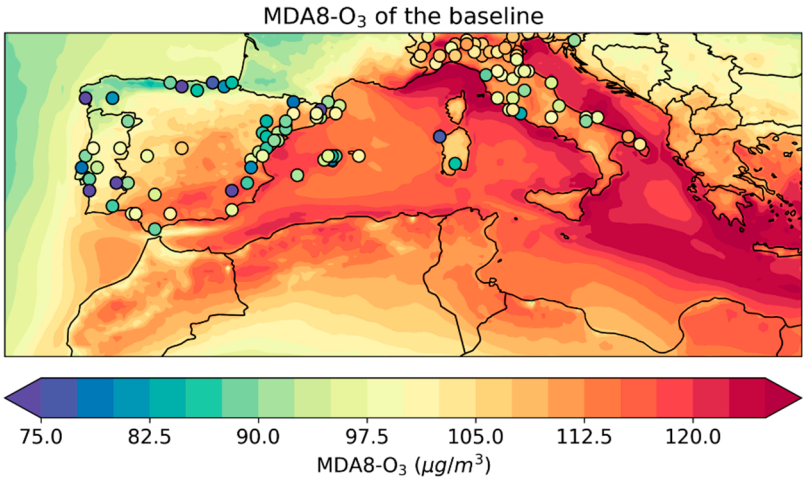

Figure 3. Daily maximum eight-hour ozone mean concentration (MDA8), averaged from April to September 2021 of the baseline model simulation. Observed values are shown with dots.

For Portugal, the baseline model simulation shows a lower MDA8 of O_3 in the Northwestern and Western parts of the country and higher values in the South. The comparison with the observed MDA8 of O_3 shows an overestimation of the modelled values by 4.6 $\mu g/m^3$ to 34.2 $\mu g/m^3$. Three stations show a higher than 17 $\mu g/m^3$ difference between the baseline simulation and the observations. One is located north of Lisbon, another is near Sines (south of Lisbon at the coast), which has a large port area, and the other is located in Alentejo, near local sources not present in the inventory. In the remaining Mediterranean area, we also see an overestimation of the model simulation ranging from 1 to 40 $\mu g/m^3$. These results agree with other modelling studies over different regions in the Mediterranean region [14,42,45], showing that the overestimation of simulated O_3 concentrations is common to many different air quality models.

3.2. Changes in the Ozone Deposition Using the Updated Vegetation Parameters

The results of the sensitivity tests (performed according to the methodology described in Section 2.2) are first explored for the ozone deposition velocity. Figure 4 shows the distribution of the mean ozone deposition velocity across the Mediterranean for the baseline run (top) and the percentage difference between the baseline and the all-changes run (below). Here, the effective deposition velocity is computed for each time step as the ratio between deposition flux ($\mu g/m^{-2}s^{-1}$) and concentration ($\mu g/m^3$) in each model grid cell and afterwards averaged across the study period (V_d = F/C). In urban areas with very low mean O_3 concentrations, this leads to very high effective V_d values, which is an artefact of the method used to derive the effective V_d over the whole study area. This occurs through a combination of low mean ozone levels due to (night time) ozone titration and deposition fluxes driven by day time conditions.

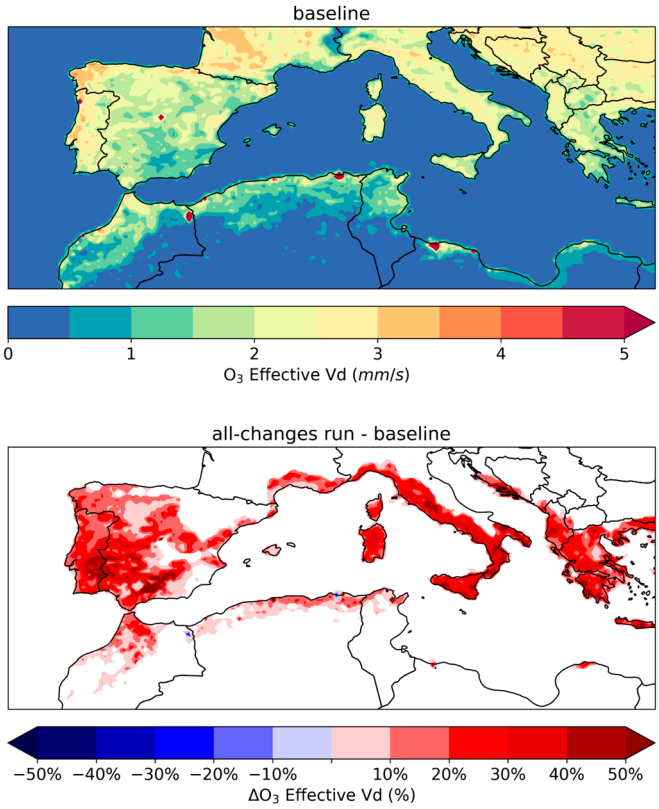

Figure 4. Ozone deposition velocity, averaged over the modelling period, of the baseline simulation (**top**) and percentage change in the all-changes run to the baseline (**below**).

The adaptations made for the Mediterranean climate for the vegetation parameters g_{max}, f_{VPD}, and f_{temp} lead to vegetation stomata staying open for more extended periods, thus increasing the stomatal deposition rates of ozone over the Mediterranean climate zone. Figure 4 shows that the deposition velocity increases in the whole Mediterranean area when the new climate zone-specific vegetation parameters are considered. The largest change in the deposition velocity has been simulated in southern Spain, an area predominantly characterized by crops and arable land. As shown in Table 1, these two land use classes experienced substantial changes in values for VPD and g_{max}. For Portugal, the changes are in the range of 10 to 40%. The largest difference has been registered in the Alentejo region near to the border with Spain, in an area mostly classified as crops and arable land. For NO_2, we observed a similar effective V_d distribution to that we have seen for O_3, with the same regions registering the largest changes (see Supplementary Materials).

Table 2 shows the modelled V_d values and the percentage difference between the sensitivity runs and the baseline model at the two Portuguese stations chosen for the analysis (Section 2.4). The two stations, which are located in grid cells mainly composed of the land classes of CRP and ARA, show an increase of 20.6% and 26.3% for the all-changes sensitivity run. The individual sensitivity runs show that CRP-g_{max} caused an increase of 12.1% at the LNH station and 10.5% at the SCO station, and thus show the same signal as the all-changes run, albeit with lower values. The lower values can be explained by the percentage of each cell covered by this land use (see Supplementary Materials). The individual sensitivity runs for arable land showed only a slight change in the deposition velocity, with ARA-g_{max} and ARA-VPD having the highest percentage change for LNH and SCO, respectively.

Table 2. Value and percentage change in ozone deposition velocity between the baseline and the all-changes runs at the Lourinhã (LNH) and Santa-Combinha (SCO) air quality stations.

		V_d (mm/s)			
Test		**LNH**		**SCO**	
Baseline		3.62	-	2.06	-
ARA	*VPD*	3.64	0.6%	2.11	2.4%
ARA	*Temp*	3.61	−0.3%	2.06	0.0%
ARA	g_{max}	3.73	3.0%	2.09	1.5%
FBD	*VPD*	3.62	0.0%	2.06	0.0%
FBD	*Temp*	3.61	−0.3%	2.06	0.0%
FBD	g_{max}	3.93	8.6%	2.15	4.4%
CRP	*VPD*	3.65	0.8%	2.15	4.4%
CRP	*Temp*	3.55	−1.9%	2.04	−1.0%
CRP	g_{max}	4.09	13.0%	2.25	9.2%
FCE	*VPD*	3.63	0.3%	2.06	0.0%
FCE	*Temp*	3.62	0.0%	2.06	0.0%
FCE	g_{max}	3.63	0.3%	2.07	0.5%
All-changes		4.43	22.4%	2.55	23.8%

Several studies show that ozone dry deposition has been underestimated in the Mediterranean climate zone (e.g., [46,47]).

3.3. Change in the Modelled Ozone Concentration

Figure 5 shows the percentage difference in average MDA8 for ozone between the model simulation performed with all changes and the baseline run (see Figure 3). As expected, the decreasing O_3 concentrations show high spatial correlation with the increase in dry deposition velocity V_d (see Figure 4). The largest changes have been calculated in the Iberian Peninsula and Italy, with values reaching −8%. Through atmospheric transport, the O_3 levels in adjacent areas, such as over the sea, are lower as well. For NO_2, an overall decrease in concentration has been modelled, although the change observed is smaller than for O_3 (see Supplementary Materials).

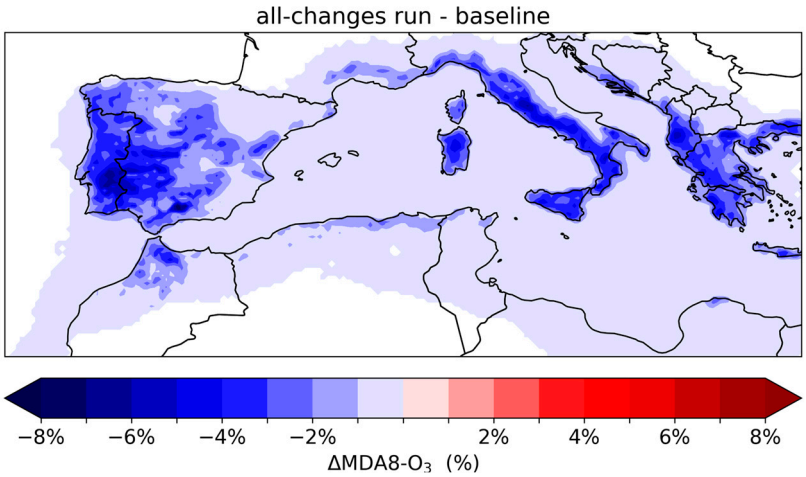

Figure 5. Percentage change in MDA8 ozone concentration between the baseline and the all-changes runs.

Figure 6 shows the scatter plot between modelled and observed average MDA8 concentration from April to September 2021. The blue symbols refer to the all-changes run, while the orange symbols represent the baseline. The regression lines were also plotted, and the Pearson correlation coefficients between the modelled and observed values were calculated. The modelled values can be read along the *y*-axis, while the *x*-axis refers to the observed concentrations. Figure 6 shows that the baseline run overestimates the ozone concentration in the rural background for most of the stations (115 out of 117). Only two stations, one located in Portugal and the other in Italy, show an underestimation of ozone. The spatial correlation is moderate, with a value of about 0.57. The modelled NO_2 concentration is on average lower than the observed concentration for most of the stations (71 out of 106). This is true for the baseline and the updated configuration. Both model setups show a spatial correlation of 0.72. These results are in agreement with previous modelling studies, such as [48,49], who also found an overall overestimation of O_3 and an underestimation of NO_2 at background sites in the Mediterranean.

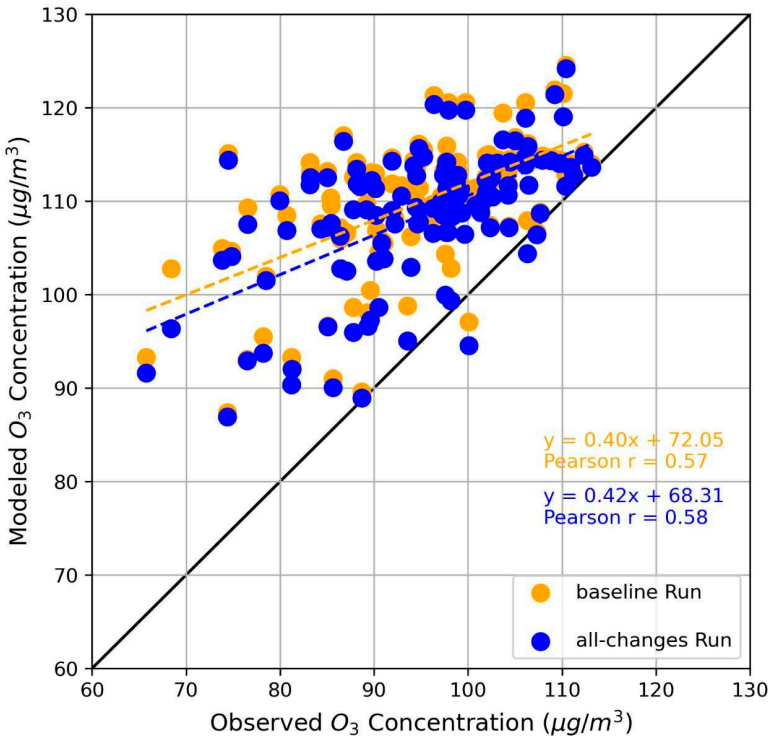

Figure 6. MDA8-O_3, averaged from April to September 2021 for all rural background stations in the Mediterranean. The spatial correlation between the modelled values and the observations are shown in the legend.

The overestimation of the model is systematically reduced for the simulation with the parameters adapted towards a Mediterranean climate. The regression analysis indicates improved statistics compared to the baseline run. The adaptation of the parameters shows a small improvement in the reduction in the bias, although a large overestimation remains for most locations. The Pearson correlation, RMSE, and bias at each individual observation site using MDA8-O_3 values were also calculated. The statistics can be read from Table S1 in the Supplementary Materials. At most stations, the analysis shows satisfying temporal correlations of 0.5 to 0.8, comparable to other model studies (e.g., [49]). The RMSE and bias are improved for the all-changes run compared to the baseline at the majority of the stations (114 out of 117).

The results are also presented for two Portuguese example sites (see Table 3, Figures 7 and 8). Table 3 lists the values for the station average MDA8-O_3 for all runs

and its percentage change from the baseline model simulation. At the two locations, the MDA8-O_3 is about 2 to 3% lower in the all-changes run than in the baseline. g_{max} was noted as the most impactful parameter for both locations, especially for the CRP land use. For the SCO station, the changes in the VPD had a noticeable impact, especially on ARA and CRP land uses.

Table 3. Value and percentage change in MDA8 ozone between the baseline and the sensitivity runs at the Lourinhã (LNH) and Santa-Combinha (SCO) air quality stations.

		O_3 Concentration (μg/m^3)			
Test		**LNH**		**SCO**	
Baseline		95.5	-	100.4	-
ARA	*VPD*	95.4	−0.1%	100.1	−0.3%
ARA	*Temp*	95.5	0.0%	100.4	0.0%
ARA	g_{max}	95.3	−0.2%	100.3	−0.1%
FBD	*VPD*	95.5	0.0%	100.4	0.0%
FBD	*Temp*	95.5	0.0%	100.5	0.1%
FBD	g_{max}	94.8	−0.7%	99.8	−0.6%
CRP	*VPD*	95.4	−0.1%	99.8	−0.6%
CRP	*Temp*	95.6	0.1%	100.6	0.2%
CRP	g_{max}	94.8	−0.7%	99.5	−0.9%
FCE	*VPD*	95.5	0.0%	100.4	0.0%
FCE	*Temp*	95.5	0.0%	100.5	0.1%
FCE	g_{max}	95.4	−0.1%	100.3	−0.1%
All-Changes		93.7	−1.9%	97.3	−3.1%

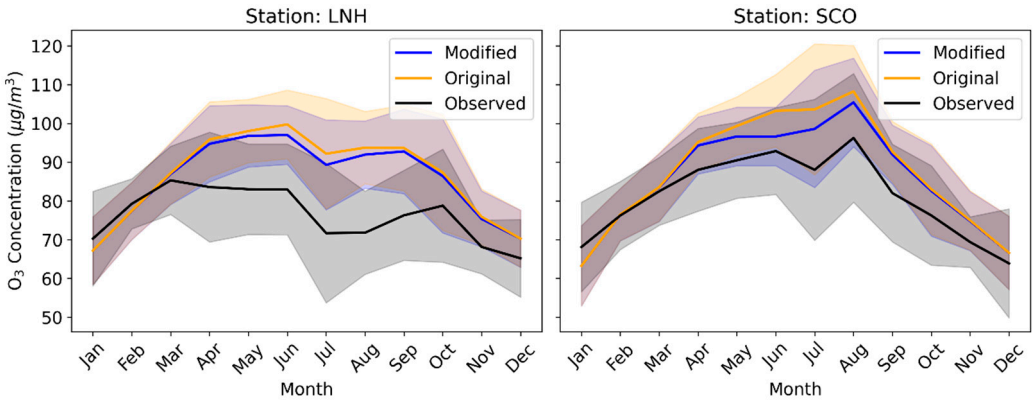

Figure 7. Monthly average (solid lines) and standard deviation (shaded area) of the MDA8-O_3 for Lourinhã (LNH) and Santa-Combinha (SCO) stations.

Figure 7 shows the monthly mean MDA8-O_3 (solid lines) and standard deviation (shaded area) of the MDA8-O_3 for the observations, the baseline and the all-changes simulation at the stations LNH and SCO. In LNH, the highest monthly mean MDA8-O_3 are observed in spring, which is typical for background sites at midlatitudes of the northern hemisphere [50,51]. SCO also exhibits high spring monthly mean values of the MDA8-O_3 (~90 μg/m^3); however, the summer peak, driven by enhanced photochemical pollution, is more pronounced. The model reproduces the different seasonality between the two stations.

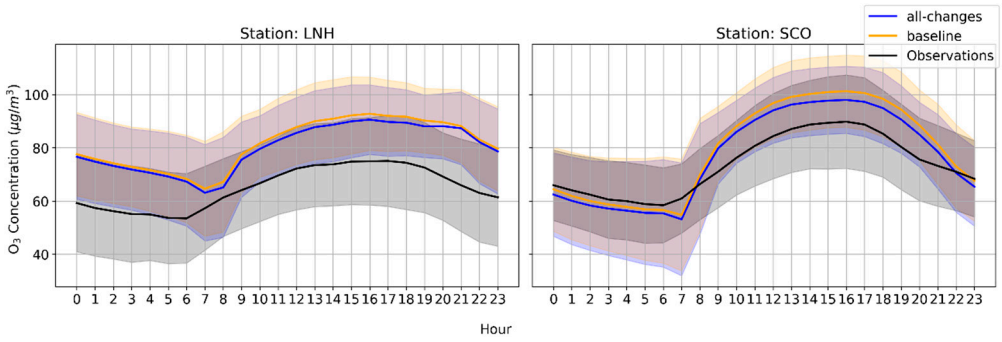

Figure 8. Diurnal cycle of the ozone concentration for the period between April and September at Lourinhã (LNH) and Santa-Combinha (SCO). The shaded area refers to the standard deviation of the observations and the two model simulations.

The baseline run follows a similar annual cycle as the observed data and captures the decrease registered in July for both stations. However, for both stations, the baseline run shows a significant overestimation, reaching up to 15 $\mu g/m^3$ during summertime. As the baseline simulation, the all-changes run follows the observations well in time but shows a reduced overestimation. As expected, the differences between baseline and all-changes run mainly appear within the April to September period, which coincides with the warmer and drier months during the growing season.

Figure 8 shows the diurnal cycle (solid lines) and standard deviation (shaded areas) for the observations, the baseline simulation and the all-changes run at the two Portuguese stations. Both stations show a similar diurnal cycle with lower observed concentrations during night time and higher observed concentrations during the day when photochemical O_3 production is taking place. At LNH, the baseline run shows a similar temporal evolution as the observations. However, the values are overestimated by up to 18 $\mu g/m^3$ throughout the day. At the more remote station, SCO, the model shows a slight underestimation during night time. The modelled concentration shows a faster increase after sunrise and thus overestimates the observations by up to 13 $\mu g/m^3$ during day time. SCO is located in the north of Portugal in a less populated area, and the diurnal cycle in the ozone concentration can be well captured by the model running at a 21 $\times$ 21 km^2 resolution. LNH is located on the coast, closer to cities and ports, in a region with higher anthropogenic emissions. This explains that the diurnal cycle in LNH is not as well captured as in SCO. Several studies have pointed out (e.g., [52]) that coarser model resolutions would not be able to capture some atmospheric dynamics, such as night time ozone titration. Thürkow et al. [22] performed a multi-model intercomparison between four regional CTMs for Germany, and they also found that rural background stations showed a better performance than urban background stations due to the model's issues with capturing night time depletion of O_3 due to titration. For the present work, the model resolution may be too coarse to capture night time ozone titration. For NO_2, the rural station SCO shows an overestimation during the night time and an accurate representation during the day. For the Mem Martins urban station (MEM), it is possible to see that the model overestimates concentrations during the morning rush hour. The different model setups caused only a slight change in the concentration at these stations. For more information, see the Supplementary Materials.

Despite the use of adapted vegetation parameters within the dry deposition routines, LOTOS-EUROS still shows an overestimation of the observed O_3 concentration in the Mediterranean, including Portugal. Elevated modelled ozone concentrations in southern European areas are not a specific problem of LOTOS-EUROS, but are also found in other modelling studies [14,48,49,53–55]. Im et al. [56] reported that lower MDA8-O_3 values were overestimated by more than 40%. The authors attribute this overestimation to

chemical boundary conditions used in the CTMs. They point to a study performed by Giorgano et al. [57], in which the influence of boundary conditions on modelling various species was analysed.

Escudero et al. [23] found that by increasing the number of vertical model layers, the performance of LOTOS-EUROS on surface ozone concentrations can be improved. Moreover, the authors found that runs with coarser spatial resolution had a disproportionate O_3 increase in the noon hours for low-wind-speed areas.

Furthermore, several studies attribute part of the ozone overestimation to emission inventory inaccuracies in representing ozone precursor emissions, especially inaccuracies in NOx emissions from traffic and industrial sources [53,58,59] and VOC emissions [54,60]. These discrepancies mean that inaccuracies in representing NOx and VOC emissions can affect the modelled NOx-to-VOC ratios, thus changing photochemical reaction rates by either enhancing ozone production in NOx-limited conditions or diminishing titration in NOx-saturated environments, leading to an overestimation of ozone concentrations.

Finally, several recent studies highlight that iodine released from dust or seawater may effectively deplete O_3 [61], with implications for surface ozone concentrations in the Mediterranean [62,63], which is not considered in our models, as iodine speciation and its phase partitioning are not included [64].

4. Conclusions

This paper aimed to improve the performance of the LOTOS-EUROS modelling system in simulating ozone over Portugal by adjusting the deposition rates in the Mediterranean climate zone and, in parallel, develop a first working version of an improved Mediterranean deposition module for LOTOS-EUROS. Vegetation parameters for four land use classes were chosen to conduct model sensitivity tests. The analysis focused on ozone concentration and deposition between April and September 2021 for a baseline run and a model simulation incorporating all the changes to the studied parameters (all-changes run).

Results for the baseline run showed a widespread overestimation of the observed maximum daily eight-hour average of ozone values. This overestimation was also found in other model studies over the Mediterranean area pointing at a number of possible reasons as discussed in Section 3.3. The changes in the dry deposition routines for the Mediterranean climate zones have reduced the overestimation of LOTOS-EUROS in simulating ozone concentrations. An improvement in the RMSE and bias for the all-changes run was noted at 9 out of 10 Portuguese stations and at 114 out of the 117 stations spread over the whole Mediterranean area, respectively. For NO_2, the model showed an underestimation of observed values at the majority of the stations. The changes made in the deposition description increased the NO_2 deposition, although this increase only resulted in a slight decrease in NO_2 concentrations.

Our study illustrates that the level of detail in the dry deposition scheme may also affect the observed bias and that further attention to this process is required. Hence, multiple steps are required to reduce the overestimation of ozone levels in the Mediterranean by current CTMs.

This study showed that detailing the dry deposition parameterization is worthwhile for reducing the biases and that additional effort will be put in by detailing further to enhance the accuracy of O_3 modelling, providing a more robust basis for assessing the impacts of O_3 on human health, crop production, and natural ecosystems in Portugal and the Mediterranean region as a whole. This will be achieved by increasing the number of land use classes and extending the adaptation of the parameter settings to these classes. Moreover, the impacts of these changes not only affect ozone but also other pollutants.

The impact of these changes on ammonia and other N-compounds will be the subject of future studies.

Supplementary Materials: The following supporting information can be downloaded at: https://www.mdpi.com/article/10.3390/atmos16050620/s1, Figure S1: Percentage change in ozone deposition velocity between the CRP-gmax run and the baseline (below); Figure S2: Percentage change in MDA8 ozone concentration between the CRP-g_{max} run and the baseline (below); Figure S3: NO_2 concentration, averaged over the modelling period, of the baseline simulation (top) and percentage change in the all-changes run to the baseline (below); Figure S4: NO_2 deposition velocity, averaged over the modelling period, of the baseline simulation (top) and percentage change in the all-changes run to the baseline (below); Figure S5: NO_2 concentration, averaged from April to September 2021 for all rural background stations in the Mediterranean. The spatial correlation between the modelled values and the observations are shown in the legend; Figure S6: Diurnal cycle of the NO_2 concentration for the period between April and September at Santa-Combinha (SCO), a rural background station, and Mem Martins (MEM), an urban background station near Lisbon. The shaded area refers to the standard deviation of the observations and the two model simulations; Table S1: Air quality station and location, correlation, RMSE, and bias for the baseline and all-changed run. Statistics calculated for MDA8 of ozone for the period of April to September 2021; Table S2: Air quality station, correlation, RMSE and bias for the baseline and all-changed run. Statistics calculated for mean NO_2 for the period of April to September 2021.

Author Contributions: Conceptualization, A.B., S.B., M.S. and A.M.; Methodology, A.B., S.B., M.T., C.G., and E.D.; Software, A.B., M.T. and M.R.; Validation, A.B. and C.G.; Formal Analysis, A.B., S.B., M.T., M.R. and A.M.; Investigation, A.B.; Resources, M.R. and A.M.; Data Curation, A.B. and C.G.; Writing—Original Draft Preparation, A.B.; Writing—Review and Editing, A.B., S.B., M.T., M.R., C.G., M.S. and A.M.; Visualization, A.B., S.B. and M.T.; Project Administration, A.M.; Funding Acquisition, S.B., C.G., M.R., M.S. and A.M. All authors have read and agreed to the published version of the manuscript.

Funding: Thanks are due to the FONDA project (Grant agreement 101079134) funded by the European Union's Horizon Europe research and innovation programme and the National Funds through the FCT–Fundação para a Ciência e Tecnologia for UID Centro de Estudos do Ambiente e Mar (CESAM) + LA/P/0094/2020, and for the contract grants of C. Gama (2021.00732.CEECIND, DOI: https://doi.org/10.54499/2021.00732.CEECIND/CP1659/CT0006) and M. Russo (2023.05938.CEECIND/CP2840/CT0010, DOI: https://doi.org/10.54499/2023.05938.CEECIND/CP2840/CT0010).

Institutional Review Board Statement: Not applicable.

Informed Consent Statement: Not applicable.

Data Availability Statement: The raw data supporting the conclusions of this article will be made available by the authors on request.

Conflicts of Interest: The authors declare no conflicts of interest.

References

1. Zhang, J.J.; Wei, Y.; Fang, Z. Ozone pollution: A major health hazard worldwide. *Front. Immunol.* **2019**, *10*, 2518. [CrossRef] [PubMed]
2. Orellano, P.; Reynoso, J.; Quaranta, N.; Bardach, A.; Ciapponi, A. Short-term exposure to particulate matter (PM_{10} and $PM_{2.5}$), nitrogen dioxide (NO_2), and ozone (O_3) and all-cause and cause-specific mortality: Systematic review and meta-analysis. *Environ. Int.* **2020**, *142*, 105876. [CrossRef] [PubMed]
3. Nuvolone, D.; Petri, D.; Voller, F. The effects of ozone on human health. *Environ. Sci. Pollut. Res.* **2018**, *25*, 8074–8088. [CrossRef]
4. Li, X.; Chen, Q.; Zheng, X.; Li, Y.; Han, M.; Liu, T.; Xiao, J.; Guo, L.; Zeng, W.; Zhang, J.; et al. Effects of ambient ozone concentrations with different averaging times on asthma exacerbations: A meta-analysis. *Sci. Total Environ.* **2019**, *691*, 549–561. [CrossRef]

5. Feng, Z.; De Marco, A.; Anav, A.; Gualtieri, M.; Sicard, P.; Tian, H.; Fornasier, F.; Tao, F.; Guo, A.; Paoletti, E. Economic losses due to ozone impacts on human health, forest productivity and crop yield across China. *Environ. Int.* **2019**, *131*, 104966. [CrossRef]
6. Jakovljević, T.; Lovreškov, L.; Jelić, G.; Anav, A.; Popa, I.; Fornasier, M.F.; Proietti, C.; Limić, I.; Butorac, L.; Vitale, M.; et al. Impact of ground-level ozone on Mediterranean forest ecosystems health. *Sci. Total Environ.* **2021**, *783*, 147063. [CrossRef] [PubMed]
7. Fischer, E.M.; Schär, C. Consistent geographical patterns of changes in high-impact European heatwaves. *Nat. Geosci.* **2010**, *3*, 398–403. [CrossRef]
8. Millán, M.M.; José Sanz, M.; Salvador, R.; Mantilla, E. Atmospheric dynamics and ozone cycles related to nitrogen deposition in the western Mediterranean. *Environ. Pollut.* **2002**, *118*, 167–186. [CrossRef]
9. Cristofanelli, P.; Bonasoni, P. Background ozone in the southern Europe and Mediterranean area: Influence of the transport processes. *Environ. Pollut.* **2009**, *157*, 1399–1406. [CrossRef]
10. Otero, N.; Sillmann, J.; Schnell, J.L.; Rust, H.W.; Butler, T. Synoptic and meteorological drivers of extreme ozone concentrations over Europe. *Environ. Res. Lett.* **2016**, *11*, 024005. [CrossRef]
11. Alonso, C.; Gouveia, C.M.; Santos, J.A. Analysis of tropospheric ozone concentration and their predictors in mainland Portugal. *Atmos. Res.* **2025**, *314*, 107766. [CrossRef]
12. Barros, N.; Fontes, T.; Silva, M.P.; Manso, M.C.; Carvalho, A.C. Analysis of the effectiveness of the NEC Directive on the tropospheric ozone levels in Portugal. *Atmos. Environ.* **2015**, *106*, 80–91. [CrossRef]
13. Ascenso, A.; Gama, C.; Blanco-Ward, D.; Monteiro, A.; Silveira, C.; Viceto, C.; Rodrigues, V.; Rocha, A.; Borrego, C.; Lopes, M.; et al. Assessing douro vineyards exposure to tropospheric ozone. *Atmosphere* **2021**, *12*, 200. [CrossRef]
14. Hogrefe, C.; Galmarini, S.; Makar, P.A.; Kioutsioukis, I.; Clifton, O.E.; Alyuz, U.; Bash, J.O.; Bellasio, R.; Bianconi, R.; Butler, T.; et al. A Diagnostic Intercomparison of Modeled Ozone Dry Deposition Over North America and Europe Using AQMEII4 Regional-Scale Simulations. *EGUsphere* **2025**, *2025*, 1–42.
15. Simpson, D.; Benedictow, A.; Berge, H.; Bergström, R.; Emberson, L.D.; Fagerli, H.; Flechard, C.R.; Hayman, G.D.; Gauss, M.; Jonson, J.E.; et al. The EMEP MSC-W chemical transport model – Technical description. *Atmos. Chem. Phys.* **2012**, *12*, 7825–7865. [CrossRef]
16. de Vries, W.; Schulte-Uebbing, L.; Kros, H.; Voogd, J.C.; Louwagie, G. Spatially explicit boundaries for agricultural nitrogen inputs in the European Union to meet air and water quality targets. *Sci. Total Environ.* **2021**, *786*, 147283. [CrossRef] [PubMed]
17. Duprè, C.; Stevens, C.J.; Ranke, T.; Bleeker, A.; Peppler-Lisbach, C.; Gowing, D.J.G.; Dise, N.B.; Dorland, E.; Bobbink, R.; Diekmann, M. Changes in species richness and composition in European acidic grasslands over the past 70 years: The contribution of cumulative atmospheric nitrogen deposition. *Glob. Change Biol.* **2010**, *16*, 344–357. [CrossRef]
18. Erisman, J.W.; Draaijers, G. Deposition to forests in Europe: Most important factors influencing dry deposition and models used for generalisation. *Environ. Pollut.* **2003**, *124*, 379–388. [CrossRef]
19. Manders, A.M.M.; Builtjes, P.J.H.; Curier, L.; Denier van der Gon, H.A.C.; Hendriks, C.; Jonkers, S.; Kranenburg, R.; Kuenen, J.J.P.; Segers, A.J.; Timmermans, R.M.A.; et al. Curriculum vitae of the LOTOS–EUROS (v2.0) chemistry transport model. *Geosci. Model Dev.* **2017**, *10*, 4145–4173. [CrossRef]
20. Curier, R.L.; Timmermans, R.; Calabretta-Jongen, S.; Eskes, H.; Segers, A.; Swart, D.; Schaap, M. Improving ozone forecasts over Europe by synergistic use of the LOTOS-EUROS chemical transport model and in-situ measurements. *Atmos. Environ.* **2012**, *60*, 217–226. [CrossRef]
21. Manders, A.M.M.; Van Meijgaard, E.; Mues, A.C.; Kranenburg, R.; Van Ulft, L.H.; Schaap, M. The impact of differences in large-scale circulation output from climate models on the regional modeling of ozone and PM. *Atmos. Chem. Phys.* **2012**, *12*, 9441–9458. [CrossRef]
22. Thürkow, M.; Schaap, M.; Kranenburg, R.; Pfäfflin, F.; Neunhäuserer, L.; Wolke, R.; Heinold, B.; Stoll, J.; Lupaşcu, A.; Nordmann, S.; et al. Dynamic evaluation of modeled ozone concentrations in Germany with four chemistry transport models. *Sci. Total Environ.* **2024**, *906*, 167665. [CrossRef]
23. Escudero, M.; Segers, A.; Kranenburg, R.; Querol, X.; Alastuey, A.; Borge, R.; De La Paz, D.; Gangoiti, G.; Schaap, M. Analysis of summer O3 in the Madrid air basin with the LOTOS-EUROS chemical transport model. *Atmos. Chem. Phys.* **2019**, *19*, 14211–14232. [CrossRef]
24. Petersen, A.K.; Brasseur, G.P.; Bouarar, I.; Flemming, J.; Gauss, M.; Jiang, F.; Kouznetsov, R.; Kranenburg, R.; Mijling, B.; Peuch, V.H.; et al. Ensemble forecasts of air quality in eastern China-Part 2: Evaluation of the MarcoPolo-Panda prediction system, version 1. *Geosci. Model Dev.* **2019**, *12*, 1241–1266. [CrossRef]
25. Marécal, V.; Peuch, V.H.; Andersson, C.; Andersson, S.; Arteta, J.; Beekmann, M.; Benedictow, A.; Bergström, R.; Bessagnet, B.; Cansado, A.; et al. A regional air quality forecasting system over Europe: The MACC-II daily ensemble production. *Geosci. Model Dev.* **2015**, *8*, 2777–2813. [CrossRef]
26. Peuch, V.H.; Engelen, R.; Rixen, M.; Dee, D.; Flemming, J.; Suttie, M.; Ades, M.; Agustí-Panared, A.; Ananasso, C.; Andersson, E.; et al. The Copernicus Atmosphere Monitoring Service from Research to Operations. *Bull. Am. Meteorol. Soc.* **2022**, *103*, E2650–E2668. [CrossRef]

27. Colette, A.; Andersson, C.; Manders, A.; Mar, K.; Mircea, M.; Pay, M.T.; Raffort, V.; Tsyro, S.; Cuvelier, C.; Adani, M.; et al. EURODELTA-Trends, a multi-model experiment of air quality hindcast in Europe over 1990–2010. *Geosci. Model Dev.* **2017**, *10*, 3255–3276. [CrossRef]
28. Bessagnet, B.; Pirovano, G.; Mircea, M.; Cuvelier, C.; Aulinger, A.; Calori, G.; Ciarelli, G.; Manders, A.; Stern, R.; Tsyro, S.; et al. Presentation of the EURODELTA III intercomparison exercise-evaluation of the chemistry transport models' performance on criteria pollutants and joint analysis with meteorology. *Atmos. Chem. Phys.* **2016**, *16*, 12667–12701. [CrossRef]
29. Colette, A.; Collin, G.; Besson, F.; Blot, E.; Guidard, V.; Meleux, F.; Royer, A.; Petiot, V.; Miller, C.; Fermond, O.; et al. Copernicus Atmosphere Monitoring Service—Regional Air Quality Production System v1.0. *EGUsphere* **2024**, *2024*, 1–92. [CrossRef]
30. Schaap, M.; Cuvelier, C.; Hendriks, C.; Bessagnet, B.; Baldasano, J.M.; Colette, A.; Thunis, P.; Karam, D.; Fagerli, H.; Graff, A.; et al. Performance of European chemistry transport models as function of horizontal resolution. *Atmos. Environ.* **2015**, *112*, 90–105. [CrossRef]
31. Kaiser, J.W.; Heil, A.; Andreae, M.O.; Benedetti, A.; Chubarova, N.; Jones, L.; Morcrette, J.J.; Razinger, M.; Schultz, M.G.; Suttie, M.; et al. Biomass burning emissions estimated with a global fire assimilation system based on observed fire radiative power. *Biogeosciences* **2012**, *9*, 527–554. [CrossRef]
32. EEA. *CORINE Land Cover 2018*; EEA: Copenhagen, Denmark, 2020. [CrossRef]
33. Köble, R.; Seufert, G. Novel Maps for Forest Tree Species in Europe. In Proceedings of the 8th European Symposium on the Physico-Chemical Behaviour of Air Pollutants: 'A Changing Atmosphere!', Torino, Italy, 17–20 September 2001; pp. 1–6.
34. van Zanten, M.C.; van Sauter, F.J.; Kruit, R.J.W.; van Jaarsveld, J.; van Pul, W. *Description of the DEPAC Module*; 2010; pp. 1–76. Available online: https://www.rivm.nl/bibliotheek/rapporten/680180001.pdf (accessed on 3 April 2025).
35. Erisman, J.W.; Van Pul, A.; Wyers, P. Parametrization of surface resistance for the quantification of atmospheric deposition of acidifying pollutants and ozone. *Atmos. Environ.* **1994**, *28*, 2595–2607. [CrossRef]
36. Urban, J.; Ingwers, M.; McGuire, M.A.; Teskey, R.O. Stomatal conductance increases with rising temperature. *Plant Signal. Behav.* **2017**, *12*, e1356534. [CrossRef]
37. Reynolds-Henne, C.E.; Langenegger, A.; Mani, J.; Schenk, N.; Zumsteg, A.; Feller, U. Interactions between temperature, drought and stomatal opening in legumes. *Environ. Exp. Bot.* **2010**, *68*, 37–43. [CrossRef]
38. Marchin, R.M.; Backes, D.; Ossola, A.; Leishman, M.R.; Tjoelker, M.G.; Ellsworth, D.S. Extreme heat increases stomatal conductance and drought-induced mortality risk in vulnerable plant species. *Glob. Chang. Biol.* **2022**, *28*, 1133–1146. [CrossRef] [PubMed]
39. Mills, G.; Harmens, H.; Hayes, F.; Pleijel, H.; Buker, P.; González-Fernández, I., III. MAPPING CRITICAL LEVELS FOR VEGETATION * International Cooperative Programme on Effects of Air Pollution on Natural Vegetation and Crops. Bangor, UK, 2017. Available online: http://icpvegetation.ceh.ac.uk (accessed on 3 April 2025).
40. Torre-Pascual, E.; Gangoiti, G.; Rodríguez-García, A.; Sáez De Cámara, E.; Ferreira, J.; Gama, C.; Gómez, M.C.; Zuazo, I.; García, J.A.; De Blas, M. Analysis of an intense O3 pollution episode on the Atlantic coast of the Iberian Peninsula using photochemical modeling: Characterization of transport pathways and accumulation processes. *Atmos. Chem. Phys.* **2024**, *24*, 4305–4329. [CrossRef]
41. Pires, J.C.M.; Alvim-Ferraz, M.C.M.; Martins, F.G. Surface ozone behaviour at rural sites in Portugal. *Atmos. Res.* **2012**, *104*, 164–171. [CrossRef]
42. Russo, M.A.; Gama, C.; Monteiro, A. How does upgrading an emissions inventory affect air quality simulations? *Air Qual. Atmos. Health* **2019**, *12*, 731–741. [CrossRef]
43. Sicard, P.; De Marco, A.; Troussier, F.; Renou, C.; Vas, N.; Paoletti, E. Decrease in surface ozone concentrations at Mediterranean remote sites and increase in the cities. *Atmos. Environ.* **2013**, *79*, 705–715. [CrossRef]
44. García, M.A.; Sánchez, M.L.; Pérez, I.A.; De Torre, B. Ground level ozone concentrations at a rural location in northern Spain. *Sci. Total Environ.* **2005**, *348*, 135–150. [CrossRef]
45. Brands, S.; Fernández-García, G.; García Vivanco, M.; Tesouro Montecelo, M.; Gallego Fernández, N.; David Saunders Estévez, A.; Enrique Carracedo García, P.; Neto Venâncio, A.; Melo Da Costa, P.; Costa Tomé, P.; et al. An exploratory performance assessment of the CHIMERE model (version 2017r4) for the northwestern Iberian Peninsula and the summer season. *Geosci. Model Dev.* **2020**, *13*, 3947–3973. [CrossRef]
46. Li, Q.; Gabay, M.; Rubin, Y.; Raveh-Rubin, S.; Rohatyn, S.; Tatarinov, F.; Rotenberg, E.; Ramati, E.; Dicken, U.; Preisler, Y.; et al. Investigation of ozone deposition to vegetation under warm and dry conditions near the Eastern Mediterranean coast. *Sci. Total Environ.* **2019**, *658*, 1316–1333. [CrossRef]
47. Li, Q.; Gabay, M.; Rubin, Y.; Fredj, E.; Tas, E. Measurement-based investigation of ozone deposition to vegetation under the effects of coastal and photochemical air pollution in the Eastern Mediterranean. *Sci. Total Environ.* **2018**, *645*, 1579–1597. [CrossRef]
48. D'Elia, I.; Briganti, G.; Vitali, L.; Piersanti, A.; Righini, G.; D'Isidoro, M.; Cappelletti, A.; Mircea, M.; Adani, M.; Zanini, G.; et al. Measured and modelled air quality trends in Italy over the period 2003–2010. *Atmos. Chem. Phys.* **2021**, *21*, 10825–10849. [CrossRef]

49. Fink, L.; Karl, M.; Matthias, V.; Oppo, S.; Kranenburg, R.; Kuenen, J.; Moldanova, J.; Jutterstrom, S.; Jalkanen, J.P.; Majamaki, E. Potential impact of shipping on air pollution in the Mediterranean region–A multimodel evaluation: Comparison of photooxidants NO_2 and O_3. *Atmos. Chem. Phys.* **2023**, *23*, 1825–1862. [CrossRef]
50. Monks, P.S. A review of the observations and origins of the spring ozone maximum. *Atmos. Environ.* **2000**, *34*, 3545–3561. [CrossRef]
51. Vingarzan, R. A review of surface ozone background levels and trends. *Atmos. Environ.* **2004**, *38*, 3431–3442. [CrossRef]
52. Rodrigues, V.; Gama, C.; Ascenso, A.; Oliveira, K.; Coelho, S.; Monteiro, A.; Hayes, E.; Lopes, M. Assessing air pollution in European cities to support a citizen centered approach to air quality management. *Sci. Total Environ.* **2021**, *799*, 149311. [CrossRef]
53. Im, U.; Daskalakis, N.; Markakis, K.; Vrekoussis, M.; Hjorth, J.; Myriokefalitakis, S.; Gerasopoulos, E.; Kouvarakis, G.; Richter, A.; Burrows, J.; et al. Simulated air quality and pollutant budgets over Europe in 2008. *Sci. Total Environ.* **2014**, *470–471*, 270–281. [CrossRef]
54. Cesari, R.; Landi, T.C.; D'Isidoro, M.; Mircea, M.; Russo, F.; Malguzzi, P.; Tampieri, F.; Maurizi, A. The on-line integrated mesoscale chemistry model bolchem. *Atmosphere* **2021**, *12*, 192. [CrossRef]
55. Pernigotti, D.; Thunis, P.; Cuvelier, C.; Georgieva, E.; Gsella, A.; De Meij, A.; Pirovano, G.; Balzarini, A.; Riva, G.M.; Carnevale, C.; et al. POMI: A model inter-comparison exercise over the Po Valley. *Air Qual. Atmos. Health* **2013**, *6*, 701–715. [CrossRef]
56. Im, U.; Bianconi, R.; Solazzo, E.; Kioutsioukis, I.; Badia, A.; Balzarini, A.; Baró, R.; Bellasio, R.; Brunner, D.; Chemel, C.; et al. Evaluation of operational on-line-coupled regional air quality models over Europe and North America in the context of AQMEII phase 2. Part I: Ozone. *Atmos. Environ.* **2015**, *115*, 404–420. [CrossRef]
57. Giordano, L.; Brunner, D.; Flemming, J.; Hogrefe, C.; Im, U.; Bianconi, R.; Badia, A.; Balzarini, A.; Baró, R.; Chemel, C.; et al. Assessment of the MACC reanalysis and its influence as chemical boundary conditions for regional air quality modeling in AQMEII-2. *Atmos. Atmos. Environ.* **2015**, *115*, 371–388. [CrossRef]
58. Visser, A.J.; Boersma, K.F.; Ganzeveld, L.N.; Krol, M.C. European NO_x emissions in WRF-Chem derived from OMI: Impacts on summertime surface ozone. *Atmos. Chem. Phys.* **2019**, *19*, 11821–11841. Available online: https://acp.copernicus.org/articles/19/11821/2019/ (accessed on 3 April 2025). [CrossRef]
59. Oikonomakis, E.; Aksoyoglu, S.; Ciarelli, G.; Baltensperger, U.; Prévôt, A.S.H. Low modeled ozone production suggests underestimation of precursor emissions (especially NOx) in Europe. *Atmos. Chem. Phys.* **2018**, *18*, 2175–2198. [CrossRef]
60. Zhu, S.; Kinnon, M.; Shaffer, B.P.; Samuelsen, G.S.; Brouwer, J.; Dabdub, D. An uncertainty for clean air: Air quality modeling implications of underestimating VOC emissions in urban inventories. *Atmos. Environ.* **2019**, *211*, 256–267. [CrossRef]
61. Sarwar, G.; Gantt, B.; Schwede, D.; Foley, K.; Mathur, R.; Saiz-Lopez, A. Impact of Enhanced Ozone Deposition and Halogen Chemistry on Tropospheric Ozone over the Northern Hemisphere. *Environ. Sci. Technol.* **2015**, *49*, 9203–9211. [CrossRef]
62. Soler, R.; Nicolás, J.F.; Caballero, S.; Yubero, E.; Crespo, J. Depletion of tropospheric ozone associated with mineral dust outbreaks. *Environ. Sci. Pollut. Res.* **2016**, *23*, 19376–19386. [CrossRef]
63. Bonasoni, P.; Cristofanelli, P.; Calzolari, F.; Bonafè, U.; Evangelisti, F.; Stohl, A.; Sajani, S.Z.; van Dingenen, R.; Colombo, T.; Balkanski, Y. Aerosol-ozone correlations during dust transport episodes. *Atmos. Chem. Phys.* **2004**, *4*, 1201–1215. [CrossRef]
64. Koenig, T.K.; Volkamer, R.; Apel, E.C.; Bresch, J.F.; Cuevas, C.A.; Dix, B.; Eloranta, E.W.; Fernandez, R.P.; Hall, S.R.; Hornbrook, R.S.; et al. Ozone depletion due to dust release of iodine in the free troposphere. *Sci. Adv.* **2021**, *7*, eabj6544. [CrossRef]